JMEPEG (2021) 30:7817–7825
https://doi.org/10.1007/s11665-021-05886-y

1059-9495/$19.00

Microstructural Evolution and Mechanical Properties of $Al_{0.5}CoCrFeNi$ High-Entropy Alloy after Cold Rolling and Annealing Treatments

Armin Ghaderi, Hossein Moghanni, and Kamran Dehghani

Submitted: 16 November 2020 / Revised: 4 April 2021 / Accepted: 24 April 2021 / Published online: 16 June 2021

The present study investigated the microstructure and mechanical properties of as-cast, homogenized, cold-rolled, and annealed $Al_{0.5}CoCrFeNi$ high-entropy alloy. The microstructure is characterized by optical microscopy, XRD, and scanning electron microscopy (SEM) equipped with energy-dispersive x-ray spectroscopy (EDS). Besides, hardness is acquired by Vickers hardness testing, and tensile testing is performed at room temperature for all samples. Results indicate that the matrix and droplet-shaped phases are present in all states. However, the needle-shaped and wall-shaped phases present after homogenization. In all samples, the matrix consists primarily of Fe, Cr, Co, and Ni, while droplet-shaped phases comprise mainly Al-Ni. Moreover, needle-shaped phases are replete with Cr, Ni, Co, Al, and Fe, whereas wall-shaped phases are rich in Cr, Co, and Fe and depleted in Al-Ni. The hardness of the $Al_{0.5}CoCrFeNi$ HEA increases after homogenizing and culminates at cold-rolled to 425 H_v due to the emerging of the needle and wall-shaped phases and consequently lattice distortion. The yield strength (YS), the ultimate tensile strength (UTS), and the ductility (ε_f) of the cold-rolled specimen are about 545 MPa, 834 MPa, and 26%, respectively. The noticeable improvement in hardness and strength in cold-rolled condition demonstrates a remarkable work-hardening effect without sacrificing much ductility.

Keywords $Al_{0.5}CoCrFeNi$, cold-rolling, heat treatment, high-entropy alloys, microstructure and mechanical properties

1. Introduction

Over the years, several functional alloy systems have been developed for various designing and modern applications. A significant number of these alloys depend on a couple of prevailing elements, namely ferrous alloys, intermetallic alloys (Ref 1, 2), and bulk metallic glass alloys (Ref 3-5), to name but a few. Besides, it is well known that the fabrication and joining of alloys for different engineering components such as turbines, engines, and exhaust systems have become a problem due to produced heat attributed to friction or mechanical deformation and hot working conditions. (Ref 6-8). With this in mind, in order to fulfill these requirements, high-entropy alloys (HEAs), enjoying at least four elements in equiatomic or near-equiatomic composition with a single-phase solid solution structure, were introduced in 2004 (Ref 9, 10). HEAs have been regarded as a possible replacement for high-temperature applications (Ref 11, 12). As far as strength, elongation, impact toughness, and corrosion resistance are concerned, HEAs provide similar or better properties than commercial materials at room and low temperature (Ref 13-16). Compared to traditional engineering alloys, HEAs have a wide-range-temperature application because they afford massive composition space for developing novel alloy families. They are more likely to be refrained from the strength and ductility trade-off by composition design and fabrication processes (Ref 17, 18). The mechanical properties of HEAs have been improving by all sorts of processes, namely alloying, heat treatment, and emerging nanoscale precipitations (Ref 19-23). For example, lattice distortion in refractory HEAs such as NbTaTiVZr enhanced the yield strength significantly (Ref 24), or additives like C and Al could lead to the occurrence of the serrated flows phenomenon, which affects the deformation behavior of HEA (Ref 25). Among the aforementioned enhancing processes of mechanical properties, cold-rolling integrated with subsequent annealing is a conventional way to increase and tune the mechanical properties of all materials, including HEA. As-cast alloys tend to be inappropriate for studying mechanical properties due to quite a few reasons, among which coarse microstructure and cast defects, which would develop into cracks, are of more significance. Therefore, before conducting the research, researchers usually remove cast defects and adjust microstructure by cold-rolling and/or heat treatment. P.P. Bhattacharjee et al. (Ref 26) used CoCrFeMnNi HEAs, which were homogenized, cold-rolled by 50%, and annealed for the subsequent experiment. A completely recrystallized CoCrFeMnNi HEAs with diverse grain sizes were successfully achieved by Sun et al. (Ref 27). As the research object, Ma et al. (Ref 28) and Tong Guo et al. (Ref 29) utilized homogenized, cold-rolled, and annealed $Al_{0.6}CoCrFeNi$, $Al_{0.5}CoCrFeNi$, respectively. In general, the HEAs which are FCC are soft and ductile (Ref 30, 31), while the HEAs which are BCC are hard and brittle (Ref 31, 32). Among studied HEAs,

Armin Ghaderi and Hossein Moghanni Contributed equally to this work as first authors.

Armin Ghaderi, Hossein Moghanni, and **Kamran Dehghani**, Department of Materials and Metallurgical Engineering, Amirkabir University of Technology (Tehran Polytechnic), Tehran, Iran. Contact e-mail: ghaderiarmin5@gmail.com.

the AlCoCrCuFeNi is an interesting system which has a wide range of microstructures and properties (Ref 33), and the effects of additive elements on microstructure and properties at room or elevated temperature have been thoroughly investigated (Ref 33, 34). $Al_{0.5}$CoCrFeNi HEA with favorable properties such as high work hardening (Ref 29), elevated temperature strength(Ref 35), as well as high corrosion and oxidation resistance (Ref 36, 37) were investigated to elucidate the phenomena exhibited in high-entropy alloys. $Al_{0.5}$CoCrFeNi HEA enjoys both ductility and strength due to its peculiar attributes. Therefore, the $Al_{0.5}$CoCrFeNi HEA has been extensively studied thanks to its outstanding properties and the fantastic prospect of application. While cold-rolling integrated with subsequent annealing plays a key role in adjusting microstructures and improving mechanical properties (Ref 38, 39), a detailed study of the influence of cold-rolling coupled with subsequent annealing on HEAs is still absent. Also, the $Al_{0.5}$CoCrFeNi HEA has not been thoroughly studied simultaneously in four different conditions. Therefore, having undergone four different states, the $Al_{0.5}$CoCrFeNi HEA was scrutinized to understand the associated changes in the microstructure and the mechanical properties. The primary novelties and objectives of this study may be summarized as:

- Inspecting the effects of four different states on the microstructure of the $Al_{0.5}$CoCrFeNi HEA
- Evaluating mechanical properties of $Al_{0.5}$CoCrFeNi HEA in four conditions

2. Materials and Methods

In this work, HEA ingots weighing about 300 g with dimensions of 12 mm(t) × 25 mm (w) × 140 mm (l) and using pure metals(higher than 99.5 wt.%) were fabricated via vacuum arc remelting (VAR) technique supplied by ALD Vacuum Technologies GmbH under a 4×10^{-5} torr vacuum. All ingots were remelted at least five times so as to enhance the homogeneity of ingots. Also, to make up for the evaporation of Al due to its relatively high vapor pressure, an additional Al (10 wt. %) was applied to each ingot. In an argon atmosphere, the as-cast ingots were homogenized at 1100 °C for 24 h to increase the homogeneity of alloying elements, followed by furnace cooling. Afterward, samples cold-rolled by 60 % in reduction, and subsequent annealing at 1100 ° C for 1 h, followed by air-cooling. Table 1 shows the chemical composition of the studied alloy using a Philips X Unique II XRF machine, close to the nominal composition of $Al_{0.5}$CoCrFeNi, and Fig. 1 summarizes thermomechanical processes used to prepare specimens. All samples were ground to 1500 grit silicon carbide papers and then mechanically polished as well as etched with Kalling's reagent (100 mL C_2H_5OH, 5 g $CuCl_2$, 100 mL HCl). The microstructure was examined by optical microscopy, XRD, and scanning electron microscopy (SEM) equipped with energy-dispersive X-ray spectroscopy (EDS) to analyze the chemical composition. The crystalline structure of samples was identified by a Rigaku Ultima IV x-ray diffractometer with Cu_{Ka} radiation and a graphite monochromator at 40 kV and 40 mA in the 2θ range of 20° to 120°, with a step size of 0.02° and a scan step time of 1 s. Also, quantitative analysis of XRD was carried out through X'Pert HighScore Plus software. A Vickers hardness tester measured the hardness of investigated alloy with a load of 30 kg and a holding time of 15 s before unloading, according to ASTM E92. The average hardness for each sample was determined from at least five measurements. Shimadzu AG-25TC tensile was employed at an engineering strain rate of 10^{-3} s^{-1} to assess the tensile properties of specimens in different conditions (Ref 40). Tensile measurements were carried out using flat dog-bone-shaped tensile samples with a gauge length of 6.9 mm and thickness of 1 mm, prepared by electrodischarge machining according to JIS Z2201 and shown in Fig. 2 (Ref 41). Having used different samples from each condition, we tested the repeatability of experimental findings.

Table 1 The chemical composition of examined alloys

Element	Al	Co	Cr	Fe	Ni
At.%	11.21	22.19	22.24	22.23	22.13

3. Results and Discussion

3.1 X-ray Diffraction of $Al_{0.5}$CoCrFeNi Alloy

Figure 3 shows the XRD pattern of $Al_{0.5}$CoCrFeNi alloy in four states: As-cast, homogenized, rolled, and annealed. All samples possess a combination of FCC and BCC crystalline forms, whereas FCC is dendritic and BCC is interdendritic. The results indicate that $Al_{0.5}$CoCrFeNi alloy in As-cast condition is primarily a FCC solid solution, whereas $Al_{0.5}$CoCrFeNi alloy in other states-cold-rolled, homogenized, and annealed- are FCC + BCC solid solution. From the major peaks, the lattice parameter of the FCC and BCC solid solutions are determined to be 0.3590 and 0.2874 nm, respectively. It can be seen from Fig. 3 that one of the primary peak intensities of the FCC, positioned in 2θ = 50.8 degree, declines significantly due to homogenization, cold rolling, and annealing treatments. On the other hand, due to the very treatments, the peak intensities of the BCC, especially that positioned in 2θ = 44.5 degrees, remarkably increase. For example, in the annealing state, the intensity of the FCC phase peaks decrease. In contrast, the intensity of the BCC phase peaks increases, indicating that a phase transformation has taken place because of the heat treatment. As a result, it is concluded that annealing treatment causes the as-cast $Al_{0.5}$CoCrFeNi alloy to eventually convert from a steady FCC structure to a BCC structure.

3.2 Microstructural Evolutions

Figures 4 and 5 show the as-cast, homogenized, cold-rolled, and annealed microstructures of studied alloy. Optical micrographs (Fig. 4) displayed a completely dendritic structure in all states, although the dendrite size was slightly different in the thickness in all states. Figure 4 shows that the interdendritic regions in as-cast and homogenized states are thicker than those in cold-rolled and annealed conditions. From microscopy observations, it is also found that the interdendritic phase emerges in a different shape: droplet shape (DSP; in every state), wall-shaped (WSP; in all samples except for as-cast

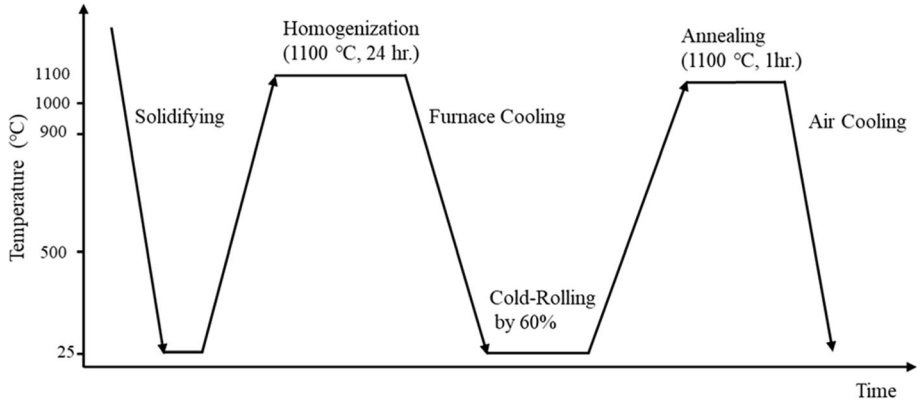

Fig. 1 Schematic diagram of thermomechanical processes used to prepare specimens

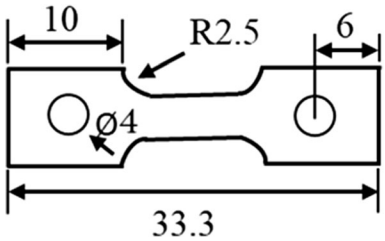

Fig. 2 The tensile specimen illustration (dimensions are in mm)

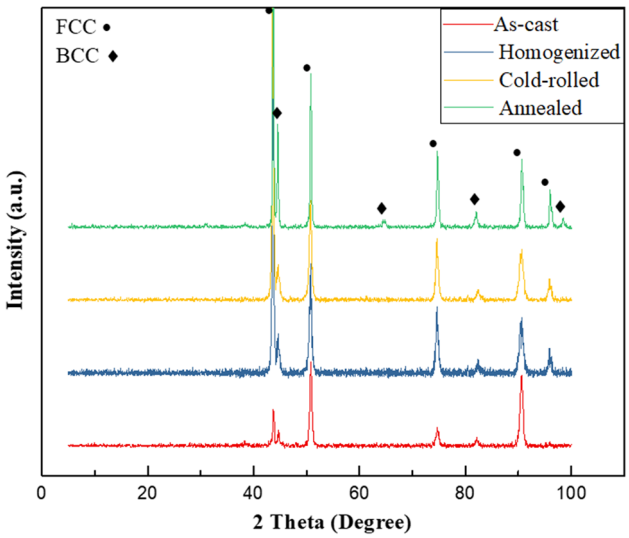

Fig. 3 XRD pattern of alloy $Al_{0.5}CoCrFeNi$ in four different conditions

sample), and needle-shaped (NSP; in all specimens with different shape except for as-cast sample).

From both microscopy and SEM observations, it is crystal clear that all samples contain the dominant dendrites and a relatively moderate amount of interdendritic regions. However, the amount of interdendritic regions in the as-cast sample is relatively small, analogous to previous research (Ref 42). In addition, by using a higher-magnification backscattered electron microscopy, Fig. 4(b) indicates a eutectic morphology in the interdendritic regions (Ref 43). Furthermore, after the as-cast state, the WSP and NSP phases start to burgeon inside the interdendritic regions and dendrite, respectively. According to Figs. 4 and 5, the significant differences between all samples are about the shape of the dendrite and interdendritic regions. In this regard, the dendritic grains are elongated along the rolling direction after cold-rolled, and the NSP phase becomes smaller and sphere-like in shape after the annealing process.

3.3 EDS Analysis

Lower melting point elements (such as Al) and eutectics tend to be segregated during liquid metal solidification and heat treatment processes. Such elemental segregation may affect mechanical, oxidation, and corrosion properties (Ref 37, 44). It is also essential to understand the amount of each element in the aforementioned regions. Elemental distribution map and chemical compositions of different phases of $Al_{0.5}CoCrFeNi$ alloy in four different states are applied and shown in Table 2 and Fig. 6. The results in all specimens indicate that the matrix consists primarily of Fe, Cr, Co, and Ni, while DSP comprises mainly Al-Ni. Moreover, NSP phases, which commence burgeoning after as-cast state in the matrix, are replete with Cr, Ni, Co, Al, and Fe, whereas WSP phases are rich in Cr, Co, and Fe and depleted in Al-Ni. (It is clearly shown in Fig. 6b, c.) The phase segregation effect happens due to the more negative mixing enthalpy of Al with other elements compared to mixing enthalpy of other atom pairs of five main elements in the system alloy (Ref 36). This effect causes different phases with different shapes and compositions. In general, during heat treatment (homogenization and annealing), the segregation of phases rich in Al-Ni and Al-(Fe, Co, Ni, Cr) is inevitable due to the aforementioned negative mixing enthalpy (Ref 45). The formation of WSPs is probably attributed to the cooling of every element to ambient temperature, giving rise to a metastable structure. However, the formation of NSPs is ascribed to the higher negative enthalpy of the phase replete with Al-Ni as well as the Al-(Ni, Cr, Co, Fe) phases compared with other sets of the five primary alloying elements (Ref 36, 46). Therefore, both Table 2 and Fig. 6 suggest that the amount of Al plays a key role in the formation and stabilization of phases, especially a BCC solid solution structure, which is analogous to previous studies (Ref 33, 42, 47, 48).

3.4 Mechanical Properties

3.4.1 Hardness of $Al_{0.5}CoCrFeNi$ Alloy in Different States. The hardness test was conducted in different regions of the four different samples, and the results are presented in

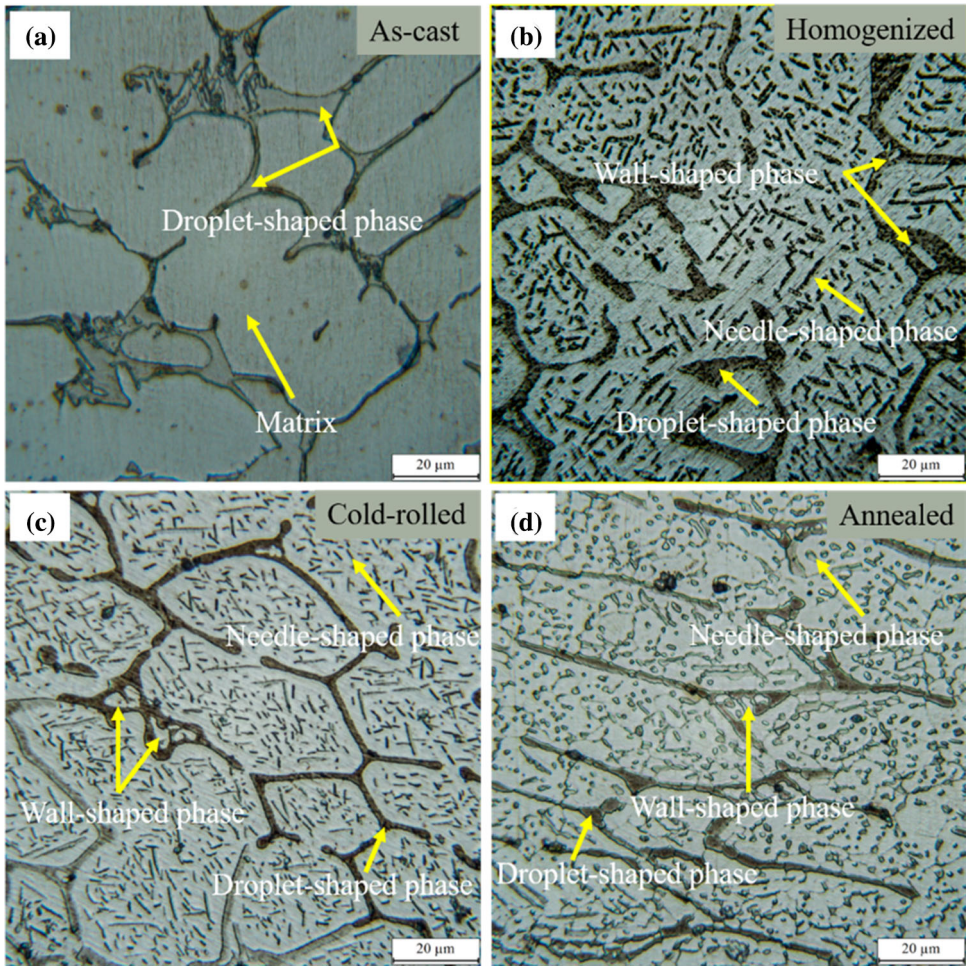

Fig. 4 Optical micrographs, related to the microstructure of $Al_{0.5}CoCrFeNi$ alloy: (a) as-cast, (b) homogenized at 1100 °C for 24 h, (c) cold-rolled by 60%, (d) annealed at 1100 °C for 1 h

Fig. 7. Results show that the hardness increases from about 155 to 230 H_V in homogenized condition. This increase might be attributed to the emergence of needle and wall-shaped phases, or it may be ascribed to lattice distortion, occurring due to the transformation of a stable FCC structure to the BCC structure. Also, these NSPs are generally acting as the second precipitation phase, and their density firmly affects the hardening process (Ref 36). Concerning the cold-rolled sample, grains are elongated in the direction of the rolling, and severe plastic deformation appears due to the 60% reduction in thickness, resulting in a sharp increase in hardness and peaking at about 425 H_V. This increase indicates a compelling work hardening occurs through cold-rolling, consistent with previous studies (Ref 29). In the annealing condition, the hardness decreases to about 250 H_V, attributing to the sparse distribution and spheroidization of the needle-shaped phase.

3.4.2 Tensile Strength of $Al_{0.5}CoCrFeNi$ Alloy in Different States. Figure 8 shows comparison of the engineering tensile curves of $Al_{0.5}CoCrFeNi$ HEAs at as-cast, homogenized, cold-rolled, and annealed conditions, and results are summarized in Table 3. The yield strength (YS), the ultimate tensile strength (UTS), and the ductility (ε_f) of the as-cast are about 294 MPa, 367 MPa, and 23%, respectively. In homogenized condition, the YS, UTS, and ε_f increase to 319 MPa, 468 MPa, and 30%, respectively. This increase can be attributed to the emerging of the wall-shaped and needle-shaped phase (shown in Figs. 4b and 5c), which increases the BCC phase structure according to Fig. 3, leading to lattice distortion. The cold-rolled specimen indicates both the high yield and ultimate tensile strength of 545 and 834 MPa, respectively. Nonetheless, the ductility does not show much decline and reaches 26%. This increase in strength without sacrificing too much plasticity might be attributed to the nano-sized B2 phase in the interdendritic region and precipitates in the dendritic region (Ref 22). However, the noticeable improvement in hardness and strength in cold-rolled condition demonstrates the effect of work hardening, reported in $Al_{0.5}CoCrFeNi$ and other HEAs (Ref 29, 49, 50). This phenomenon's key reason is activities related to dislocations, among which the density of dislocation aggregation and the creation of dislocation networks are of more consideration through the cold rolling procedure. It is well known that cold-rolling leads to the reduction of thickness and, consequently, causes dislocation proliferation, and then dislocations' interactions increase the resistance to dislocation motion in the progression of deformation. Therefore, the increase in the strength is mainly related to the density of dislocation and defined as the following equation (Ref 29):

$$\tau = \tau_0 + \alpha G b \sqrt{\rho} \qquad \text{(Eq 1)}$$

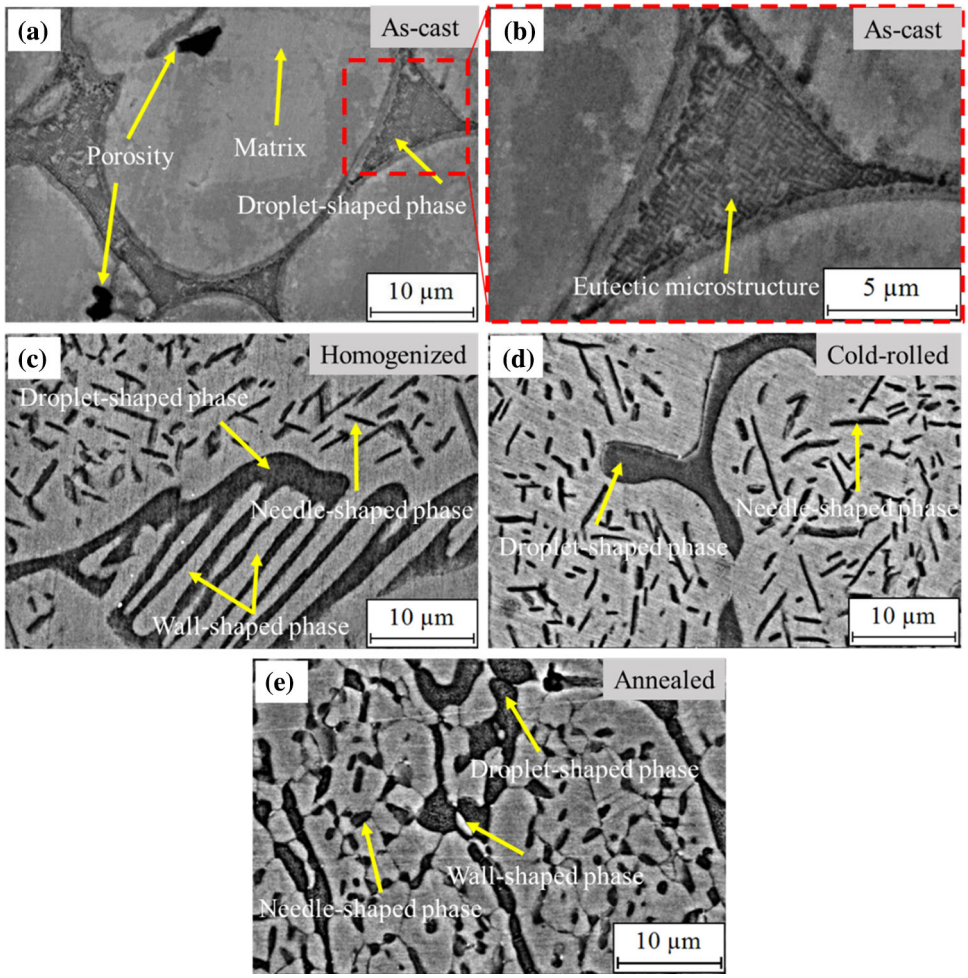

Fig. 5 SEM images, related to the microstructure of $Al_{0.5}CoCrFeNi$ alloy: (a)as-cast, (b) magnified of the interdendritic region in the as-cast state showing a eutectic microstructure, (c) homogenized at 1100 °C for 24 h, (d) cold-rolled by 60%, (e) annealed at 1100 °C for 1 h

Table 2 EDS results of phases in four different conditions

No	Spceimen name	Phase	Al	Ni	Co	Cr	Fe
			Unit, at.%				
1	As-cast	Matrix	11	22	22	23	22
		DSP	25	32	19	12	12
		WSP	…	…	…	…	…
		NSP	…	…	…	…	…
2	Homogenized	Matrix	10	23	23	22	22
		DSP	26	38	17	7	12
		WSP	15	18	21	25	24
		NSP	19	21	20	19	21
3	Cold-rolled	Matrix	9	23	24	22	22
		DSP	27	38	17	7	11
		WSP	15	16	21	26	25
		NSP	19	21	19	20	21
4	Annealed	Matrix	10	24	23	21	22
		DSP	25	35	16	10	14
		WSP	16	18	25	20	21
		NSP	14	21	23	19	23

where ρ is the dislocation density, b is the Burgers vector, G is the shear modulus, α is a constant between 0.3 and 0.6, τ_0 is the primary stress required to active a dislocation when other dislocations are not present, and τ is the flow stress. The cold-rolled $Al_{0.5}CoCrFeNi$ alloy seems to be influenced by the high density of dislocation, leading to a superior strength (Ref 51). However, the deformation twinning in other HEAs such as CoCrFeMnNi alloy is one factor for increasing the rate of work hardening and the ultimate tensile strength (Ref 15, 52). By the same token, the twining might be produced through the $Al_{0.5}CoCrFeNi$ alloy's deformation procedure and give rise to superior hardness and strength (Ref 29). As discussed before, $Al_{0.5}CoCrFeNi$ alloy in annealed condition showed significant grains refinement compared to other conditions. Thus, this capacity of $Al_{0.5}CoCrFeNi$ alloy and other HEAs could be exploited to adjust the microstructure and expand structural material with better mechanical properties by cold-rolling combined with subsequent annealing. With this in mind, the annealed sample shows high strength and ductility simultaneously (shown in Fig. 8 and Table 3). The decrease in strength and increase in ductility can be attributed to eradicating lattice distortion and strain, as well as declining dislocation densities (Ref 29).

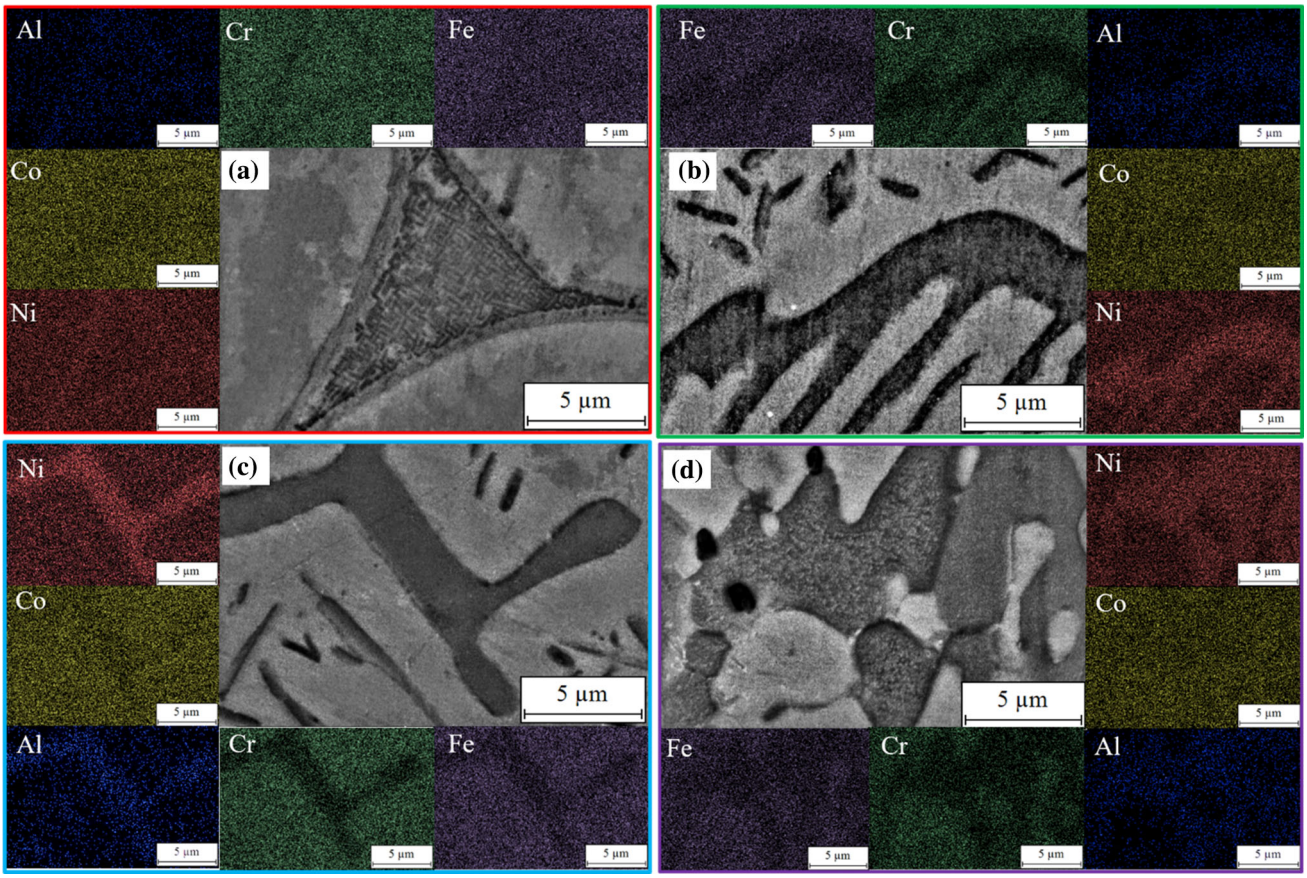

Fig. 6 BSE images and EDS maps of $Al_{0.5}CoCrFeNi$ alloy: (a) as-cast, (b) homogenized at 1100 °C for 24 h, (c) cold-rolled by 60%, (d) annealed at 1100 °C for 1 h

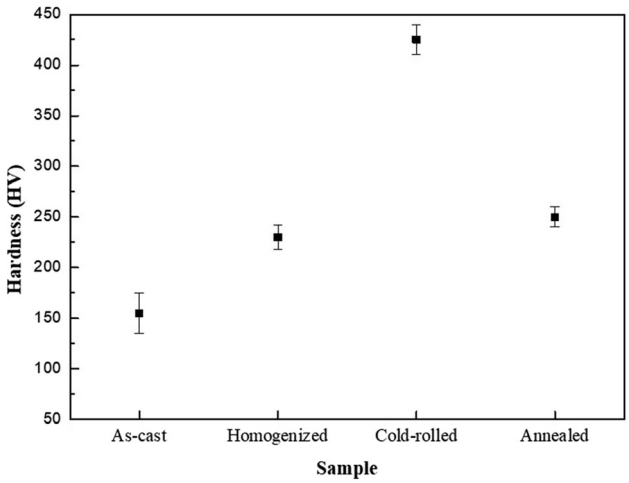

Fig. 7 The hardness of $Al_{0.5}CoCrFeNi$ alloy in different conditions

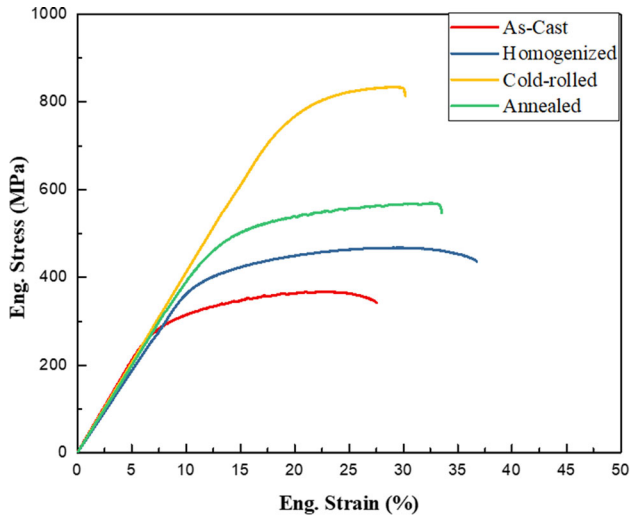

Fig. 8 Engineering tensile curves of $Al_{0.5}CoCrFeNi$ HEA in different conditions

3.5 Fractography of Fractured Samples

Figure 9 shows the typical fracture surfaces of the as-cast, homogenized, cold-rolled, and annealed sample after tensile testing. A typical dimple feature is observed in all specimens, indicating that specimens underwent considerable plastic deformation and failed in a ductile fracture mode. No trace of brittle fracture is detected on all the surfaces. As-cast sample contains large but shallow dimples, matching the moderate elongation, while homogenized and annealed specimen show large and deep dimples, signifying the substantial elongation. However, the cold-rolled sample enjoys fine dimples, and a high density of fine dimples is observed.

This work corroborates the superior mechanical properties of $Al_{0.5}CoCrFeNi$ alloy through cold-rolling and subsequent annealing. The findings provide a clear idea for the production

Table 3 Mechanical characteristics of $Al_{0.5}CoCrFeNi$ HEA in different conditions

No	Specimen name	YS, MPa	UTS, MPa	ε_f, %	Hardness, H_v
1	As-cast	294 ± 9	367 ± 12	23	155 ± 20
2	Homogenized	319 ± 10	468 ± 11	30	230 ± 12
3	Cold-rolled	545 ± 16	834 ± 13	26	425 ± 15
4	Annealed	432 ± 14	569 ± 9	28	250 ± 10

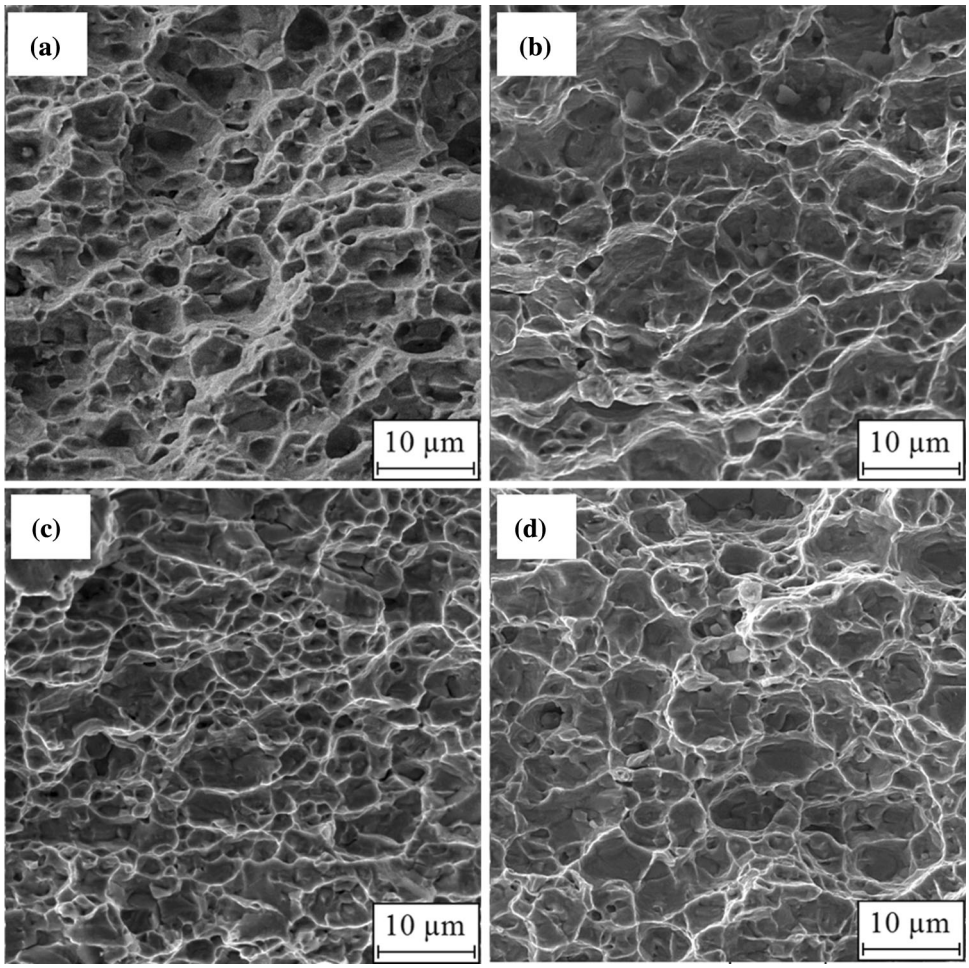

Fig. 9 SEM fractography of samples: (a) as-cast, (b) homogenized, (c) cold-rolled, (d) annealed

of HEAs. Having considered all aforementioned results and discussion and the peculiar feature of multi principal components, researchers can optimize HEAs to achieve the toughening alloys.

4. Conclusions

In this work, the $Al_{0.5}CoCrFeNi$ HEA regarding microstructure and mechanical properties is successfully investigated in four different conditions: as-cast, homogenization, cold-rolling, and annealing. The key findings can be described as follows:

- The $Al_{0.5}CoCrFeNi$ HEA in all conditions except for as-cast condition comprises four phases: matrix, droplet-shaped, needle-shaped, and wall-shaped. The as-cast sample only consists of matrix and droplet-shaped phases.
- In all specimens, the matrix contains mostly Fe, Cr, Co, and Ni, whereas droplet-shaped phases consist mainly Al-Ni. Furthermore, needle-shaped phases are rich in Cr, Ni, Co, Al, and Fe, while wall-shaped phases are rich in Cr, Co, and Fe and depleted in Al-Ni.
- The $Al_{0.5}CoCrFeNi$ HEA enjoys brilliant cold workability and can be rolled to 60% thickness reduction at room temperature without any signs of failure. The yield strength (YS), the ultimate tensile strength (UTS), the ductility (ε_f), and the hardness of the cold-rolled sample are about 545 MPa, 834 MPa, 26%, 425 H_v, respectively, signifying compelling work-hardening effect compared to other samples.

- Quite a few reasons attribute to the hardening of cold-rolling $Al_{0.5}CoCrFeNi$ HEA, namely the interaction of dislocations, twins through deformation, and lattice distortion.

References

1. G.L. Chen and C.T. Liu, Moisture Induced Environmental Embrittlement of Intermetallics, *Int. Mater. Rev.*, 2001, **46**(6), p 253–270
2. C.T. Liu and W.C. Oliver, Environmental Embrittlement and Grain-Boundary Fracture in Ni_3Si, *Scr. Metall. Mater.*, 1991, **25**, p 1933–1937
3. A. Peker and W.L. Johnson, A Highly Processable, *Appl. Phys. Lett.*, 2015, **2001**(2342), p 22–25
4. A. Inoue and A. Takeuchi, Recent Progress in Bulk Glassy, Nanoquasicrystalline and Nanocrystalline Alloys, *Mater. Sci. Eng. A*, 2004, **375–377**(1–2), p 16–30
5. N. Chen, D. Pan, D.V. Louzguine-Luzgin, G.Q. Xie, M.W. Chen and A. Inoue, Improved Thermal Stability and Ductility of Flux-Treated Pd40Ni40Si4P16 BMG, *Scr. Mater. Acta Materialia Inc.*, 2010, **62**(1), p 17–20
6. S. Praveen and H.S. Kim, High-Entropy Alloys: Potential Candidates for High-Temperature Applications–An Overview, *Adv Eng Mater*, 2017, **1700645**, p 1–22
7. A. Mashhuriazar, H. Omidvar, C.H. Gur and Z. Sajuri, Effect of Welding Parameters on the Liquation Cracking Behavior of High-Chromium Ni-Based Superalloy, *J. Mater. Eng. Perform.*, 2020, **29**(12), p 7843–7852
8. A. Ebrahimzadeh Pilehrood, H. Omidvar, A. Shamsipur and Z. Sajuri, Influence of Transient Liquid Phase Bonding Followed by Homogenization on the Fatigue Lifetimes of Inconel 738 at Elevated Temperature, *J. Manuf. Process.*, 2020, **55**, p 348–358
9. B. Cantor, I.T.H. Chang, P. Knight and A.J.B. Vincent, Microstructural Development in Equiatomic Multicomponent Alloys, *Mater. Sci. Eng. A*, 2004, **377**, p 213–218
10. J.W. Yeh, S.K. Chen, S.J. Lin, J.Y. Gan, T.S. Chin, T.T. Shun, C.H. Tsau and S.Y. Chang, Nanostructured High-Entropy Alloys with Multiple Principal Elements: Novel Alloy Design Concepts and Outcomes, *Adv. Eng. Mater.*, 2004, **6**(5), p 299–303
11. E.P. George, D. Raabe and R.O. Ritchie, High-Entropy Alloys, *Nat. Rev. Mater.*, 2019 https://doi.org/10.1038/s41578-019-0121-4
12. Y. Zhang, T. Ting, Z. Tang, M.C. Gao, K.A. Dahmen, P.K. Liaw and Z. Ping, Progress in Materials Science Microstructures and Properties of High-Entropy Alloys, *Prog. Mater. Sci.*, 2014, **61**, p 1–93
13. G. Laplanche, A. Kostka, C. Reinhart, J. Hunfeld, G. Eggeler and E.P. George, Reasons for the Superior Mechanical Properties of Medium-Entropy CrCoNi Compared to High-Entropy CrMnFeCoNi, *Acta Mater.*, 2017, **128**, p 292–303
14. B. Gludovatz, A. Hohenwarter, K.V.S. Thurston, H. Bei, Z. Wu, E.P. George and R.O. Ritchie, Exceptional Damage-Tolerance of a Medium-Entropy Alloy CrCoNi at Cryogenic Temperatures, *Nat. Commun.*, 2016, **7**, p 1–8
15. B. Gludovatz, A. Hohenwarter, D. Catoor, E.H. Chang, E.P. George and R.O. Ritchie, A Fracture-Resistant High-Entropy Alloy for Cryogenic Applications, *Science*, 2014, **345**(6201), p 1153–1158
16. Y. Qiu, S. Thomas, D. Fabijanic, A.J. Barlow, H.L. Fraser and N. Birbilis, Microstructural Evolution, Electrochemical and Corrosion Properties of Al x CoCrFeNiTi y High Entropy Alloys, *Mater. Des.*, 2019, **170**, p 107698
17. T. Yang, Y.L. Zhao, Y. Tong, Z.B. Jiao, J. Wei, J.X. Cai, X.D. Han, D. Chen, A. Hu, J.J. Kai, K. Lu, Y. Liu and C.T. Liu, Multicomponent Intermetallic Nanoparticles and Superb Mechanical Behaviors of Complex Alloys, *Science*, 2018, **362**(6417), p 933–937
18. Z. Li, K.G. Pradeep, Y. Deng, D. Raabe and C.C. Tasan, Metastable High-Entropy Dual-Phase Alloys Overcome the Strength-Ductility Trade-Off, *Nature*, 2016, **534**(7606), p 227–230. https://doi.org/10.1038/nature17981
19. H.F. Sheng and L.M. Peng, Microstructure and Tensile Properties of $Al_{0.5}CoCrcuFeNi$ High-Entropy Alloy, *Appl. Mech. Mater.*, 2014, **456**, p 494–497
20. B. Ren, J. Ma, R. Zhao, S. Guan and H. Zhang, Age Hardening of AlCrMoNiTi High Entropy Alloy Prepared by Powder Metallurgy, *Xiyou Jinshu Cailiao Yu Gongcheng/Rare Met. Mater. Eng.*, 2014, **43**(6), p 1286–1290
21. Q.H. Tang, Y. Huang, Y.Y. Huang, X.Z. Liao, T.G. Langdon and P.Q. Dai, Hardening of an $Al_{0.3}CoCrFeNi$ High Entropy Alloy via High-Pressure Torsion and Thermal Annealing, *Mater. Lett.*, 2015, **151**, p 126–129
22. A. Cocrfeni, S. Niu, H. Kou, T. Guo, Y. Zhang, J. Wang and J. Li, Author ' s Accepted Manuscript Strengthening of Nanoprecipitations in an Annealed, *Mater. Sci. Eng. A*, 2016 https://doi.org/10.1016/j.msea.2016.06.040
23. J.Y. He, H. Wang, H.L. Huang, X.D. Xu, M.W. Chen, Y. Wu, X.J. Liu, T.G. Nieh, K. An and Z.P. Lu, A Precipitation-Hardened High-Entropy Alloy with Outstanding Tensile Properties, *Acta Mater.*, 2016, **102**, p 187–196
24. C. Lee, Y. Chou, G. Kim, M.C. Gao, K. An, J. Brechtl, C. Zhang, W. Chen, J.D. Poplawsky, G. Song, Y. Ren, Y.C. Chou and P.K. Liaw, Lattice-Distortion-Enhanced Yield Strength in a Refractory High-Entropy Alloy, *Adv. Mater.*, 2020, **32**(49), p 1–9
25. J. Brechtl, S. Chen, C. Lee, Y. Shi, R. Feng, X. Xie, D. Hamblin, A.M. Coleman, B. Straka, H. Shortt, R.J. Spurling and P.K. Liaw, A Review of the Serrated-Flow Phenomenon and Its Role in the Deformation Behavior of High-Entropy Alloys, *Metals (Basel)*, 2020, **10**(8), p 1–72
26. P.P. Bhattacharjee, G.D. Sathiaraj, M. Zaid, J.R. Gatti, C. Lee, C.W. Tsai and J.W. Yeh, Microstructure and Texture Evolution during Annealing of Equiatomic CoCrFeMnNi High-Entropy Alloy, *J. Alloys Compd.*, 2014, **587**, p 544–552
27. S.J. Sun, Y.Z. Tian, H.R. Lin, X.G. Dong, Y.H. Wang, Z.J. Zhang and Z.F. Zhang, Enhanced Strength and Ductility of Bulk CoCrFeMnNi High Entropy Alloy Having Fully Recrystallized Ultrafine-Grained Structure, *Mater. Des.*, 2017, **133**, p 122–127. https://doi.org/10.1016/j.matdes.2017.07.054
28. L. Ma, L. Wang, Z. Nie, F. Wang, Y. Xue, J. Zhou, T. Cao, Y. Wang and Y. Ren, AC SC, *Acta Mater.*, 2017 https://doi.org/10.1016/j.actamat.2017.02.014
29. T. Guo, J. Li, J. Wang, W. Yi, Y. Liu, X. Luo and H. Kou, Author ' s Accepted Manuscript, *Mater. Sci. Eng. A*, 2018 https://doi.org/10.1016/j.msea.2018.05.054
30. F. Wang, Y. Zhang and G. Chen, Tensile and Compressive Mechanical Behavior of a $CoCrCuFeNiAl_{0.5}$ High Entropy Alloy, *Int. J. Modern Phys.*, 2009, **23**, p 1254–1259
31. Y. Lu, Y. Dong, S. Guo, L. Jiang, H. Kang, T. Wang, et al, A Promising New Class of High-Temperature Alloys: Eutectic High-Entropy Alloys, *Sci. Rep.*, 2014, **4**(1), p 1–5
32. C. Tsai, M. Tsai, J. Yeh and C. Yang, Effect of Temperature on Mechanical Properties of $Al_{0.5}CoCrCuFeNi$ Wrought Alloy, *J. Alloys Compd.*, 2010, **490**(1–2), p 160–165
33. C.J. Tong, Y.L. Chen, S.K. Chen, J.W. Yeh, T.T. Shun, C.H. Tsau, S.J. Lin and S.Y. Chang, Microstructure Characterization of AlxCoCrCuFeNi High-Entropy Alloy System with Multiprincipal Elements, *Metall. Mater. Trans. A Phys. Metall. Mater. Sci.*, 2005, **36**(4), p 881–893
34. C.-Y. Hsu, J.-W. Yeh, S.-K. Chen and T.-T. Shun, Wear Resistance and High-Temperature Compression Strength of Fcc CuCoNiCrAl, *Metall. Mater. Trans. A, Phys. Metall. Mater. Sci.*, 2004, **35**(5), p 1465–1469
35. Y. Zhang, J. Li, J. Wang, S. Niu and H. Kou, Hot Deformation Behavior of As-Cast and Homogenized $Al_{0.5}CoCrFeNi$ High Entropy Alloys, *Metals (Basel).*, 2016, **6**(11), p 277
36. C.M. Lin and H.L. Tsai, Evolution of Microstructure, Hardness, and Corrosion Properties of High-Entropy Al0.5CoCrFeNi Alloy, *Intermetallics*, 2011, **19**(3), p 288–294
37. S. Abbaszadeh, A. Pakseresht, H. Omidvar and A. Shafiei, Investigation of the High-Temperature Oxidation Behavior of the $Al_{0.5}CoCrFeNi$ High Entropy Alloy, *Surf. Interfaces*, 2020 https://doi.org/10.1016/j.surfin.2020.100724
38. H.Y. Yasuda, H. Miyamoto, K. Cho and T. Nagase, Formation of Ultrafine-Grained Microstructure in $Al_{0.3}CoCrFeNi$ High Entropy Alloys with Grain Boundary Precipitates, *Mater. Lett.*, 2017 https://doi.org/10.1016/j.matlet.2017.04.072
39. B. Gwalani, V. Soni, M. Lee, S.A. Mantri, Y. Ren and R. Banerjee, Optimizing the Coupled Effects of Hall-Petch and Precipitation Strengthening in a $Al_{0.3}$ CoCrFeNi High Entropy Alloy, *Mater. Des.*, 2017, **121**, p 254–260

40. S. Niu, H. Kou, Y. Zhang, J. Wang and J. Li, Author's Accepted Manuscript, *Mater. Sci. Eng. A*, 2017 https://doi.org/10.1016/j.msea.2017.05.075
41. E. Abbasi and K. Dehghani, Materials Science & Engineering A Hot Tensile Properties of CoCrFeMnNi (NbC) Compositionally Complex Alloys, *Mater. Sci. Eng. A*, 2020, **772**, p 138771. https://doi.org/10.1016/j.msea.2019.138771
42. Y. Kao, T. Chen, S. Chen and J. Yeh, Microstructure and Mechanical Property of As-Cast, -Homogenized, and -Deformed Al x CoCrFeNi (0 ≤ x ≤ 2) High-Entropy Alloys, *J Alloys Compd*, 2009, **488**, p 57–64
43. H. Azhari-Saray, M. Sarkari-Khorrami, A. Nademi-Babahadi and S.F. Kashani-Bozorg, Dissimilar Resistance Spot Welding of 6061–T6 Aluminum Alloy/St-12 Carbon Steel Using a High Entropy Alloy Interlayer, *Intermetallics*, 2020, **124**, p 106876
44. R. Sokkalingam, K. Sivaprasad, M. Duraiselvam, V. Muthupandi and K.G. Prashanth, Novel Welding of $Al_{0.5}$CoCrFeNi High-Entropy Alloy: Corrosion Behavior, *J. Alloys Compd.*, 2019 https://doi.org/10.1016/j.jallcom.2019.153163
45. C. Tsai, Y. Chen, M. Tsai, J. Yeh, T. Shun and S. Chen, Deformation and Annealing Behaviors of High-Entropy Alloy $Al_{0.5}$ CoCrCuFeNi, *J. Alloys Compd.*, 2009, **2010**(486), p 427–435
46. T. Shun and Y. Du, Age Hardening of the $Al_{0.3}CoCrFeNiC_{0.1}$ High Entropy Alloy, *J. Alloys Compd.*, 2009, **478**(1–2), p 269–272
47. Z. Tang, M.C. Gao, H. Diao, T. Yang, J. Liu, T. Zuo, Y. Zhang, Z. Lu, Y. Cheng, Y. Zhang, K.A. Dahmen, P.K. Liaw and T. Egami, Aluminum Alloying Effects on Lattice Types Microstructures, and Mechanical Behavior of High-Entropy Alloys Systems, *Jom*, 2013, **65**(12), p 1848–1858
48. Y.J. Zhou, Y. Zhang, Y.L. Wang and G.L. Chen, Solid Solution Alloys of AlCoCrFeNi Tix with Excellent Room-Temperature Mechanical Properties, *Appl. Phys. Lett.*, 2007, **90**(18), p 181904
49. Z.P. Lu, H. Wang, M.W. Chen, I. Baker, J.W. Yeh, C.T. Liu and T.G. Nieh, An Assessment on the Future Development of High-Entropy Alloys: Summary from a Recent Workshop, *Intermetallics*, 2015, **66**, p 67–76
50. O.N. Senkov and S.L. Semiatin, Microstructure and Properties of a Refractory High-Entropy Alloy after Cold Working, *J. Alloys Compd.*, 2015, **649**, p 1110–1123
51. I. Baker, F. Meng, M. Wu and A. Brandenberg, Recrystallization of a Novel Two-Phase FeNiMnAlCr High Entropy Alloy, *J. Alloys Compd.*, 2016, **656**, p 458–464
52. F. Otto, A. Dlouhy, C. Somsen, H. Bei, G. Eggeler and E.P. George, The Influences of Temperature and Microstructure on the Tensile Properties of a CoCrFeMnNi High-Entropy Alloy, *Acta Mater.*, 2013, **61**(15), p 5743–5755